ELSEVIER

Chemical Engineering Journal 77 (2000) 79–86

Chemical Engineering Journal

www.elsevier.com/locate/cej

Network analysis of filter cake pore structure by high resolution X-ray microtomography

C.L. Lin, J.D. Miller *

Department of Metallurgical Engineering, University of Utah, Salt Lake City, UT 84112, USA

Abstract

Continuous filtration of fine particles involves filter cake formation and removal of surface moisture by drawing air through the pore structure network. Conventional network theory can be used to study the phenomena of flow through a porous structure by treating the pores as discrete volumes and connecting these with pore throats as resistances of zero volume. In this regard, analysis of the pore connectivity in a packed bed of particles should allow for a detailed description of fluid flow and transport in the filter cake structure. As the resolution and the techniques for 3-D geometric analysis have advanced in the last decade, it is now possible to specify in detail the pore structure in three-dimensional digital space using high-resolution X-ray microtomography to resolve features with micrometer resolution. This paper presents preliminary experimental findings of a filter cake pore structure in 3-D using X-ray microtomographic techniques.

Keywords: Filter cake; Pore structure; X-ray microtomography

1. Introduction

Description of heterogeneous structures based on geometrical considerations is of importance in many fields of applied science and technology, including fluid flow in porous media such as occurs during fine particle filtration. Continuous filtration of fine particles involves filter cake formation and removal of surface moisture by drawing air through the porous structure. The physical laws that govern the equilibrium state and the flow of fluids through the filter cake, are simple and well known. In practice, however, only the global physical properties of the system are known at best. Unfortunately, because of the complexity of the pore geometry, it is difficult to predict macroscopic (effective) properties from microscopic (pore level) properties. In general, there is no linear or non-linear rule for the use of microscopic physical properties to predict the macroscopic scale properties. In this regard, it is essential to develop appropriate experimental techniques and theoretical models to describe in detail the flow which occurs through a packed bed during fine particle filtration.

Almost all theory related to transport phenomena in porous media leads to macroscopic laws applicable to systems whose dimensions are large compared with the dimensions of the pores. These macroscopic pore structure parameters represent average behavior of a sample containing many pores. The important macroscopic pore structure parameters important in filtration are porosity, permeability, specific surface area, formation resistivity factor and the breakthrough capillary pressure. A review of the definitions and measurement techniques for these macroscopic parameters is given by Dullien [1]. Generally speaking, the macroscopic quantity of interest is more or less influenced by the microscopic properties of the pore structure and is obtained by a spatial integration of the local field. The overall pore fraction and pore size distribution are two of the most important microscopic parameters which must be used for model development to obtain fundamental relationships between pore structure and the effective transport coefficients. Furthermore, conventional network theory can be used to study the phenomena of flow through a porous structure by treating pores as discrete volumes and connecting these with pore throats as resistances of zero volume. In this regard, network analysis of the 3-D connectivity and pore geometry is necessary to determine the effective filter cake transport properties.

Most recent methods being used to characterize the pore microstructure and its interconnected network rely on the microscopic observation of a series of thin sections or polished sections of the porous media (in our case filter cake). These data sets are then used to reconstruct and to display the three-dimensional image of the porous system with the help of advanced computer graphic techniques. Complete analy-

* Corresponding author. Tel.: +1-801-581-5160; fax: +1-801-581-8119.
E-mail address: jdmiller@mines.utah.edu (J.D. Miller).

1385-8947/00/$ – see front matter
PII: S1385-8947(99)00149-7

sis of the 3-D porous structure from serial sections is limited. As the resolution and the techniques for 3-D geometric analysis have advanced in the last decade, it is now possible to map in detail the pore structure in three-dimensional digital space using high-resolution X-ray microtomography to resolve features with micrometer resolution. A detailed description of the interconnected pore structure based on the concepts of 'connectivity', 'percolation', and 'tortuosity', needs to be developed using 3-D X-ray microtomography in order to establish fundamental relationships between complex random pore structures and the corresponding effective transport coefficients. This paper presents information on the techniques, methodology, and preliminary experimental findings for network analysis of a completely interconnected porous filter cake using X-ray microtomography.

2. Filtration theory

2.1. Classical approach

Most of the derivation is based on the work of Happel and Brenner [2]. The classical approach [3–5] for filtration analysis is based on Darcy's law, an empirical equation that describes one-dimensional fluid flow through a uniform incompressible porous media. Knowledge of cake pore microstructure and its correlation to macroscopic cake properties is required to model the filtration from a fundamental point of view. Darcy's law is defined as

$$U = \frac{Q}{A} = \frac{1}{A}\frac{\mathrm{d}V}{\mathrm{d}t} = \frac{k\Delta p}{\mu\,\ell} \tag{1}$$

where U is the fluid velocity, Q is the volume flow rate, V is the volume of the fluid, k is the permeability, μ the viscosity of the fluid, A the cross sectional area of the one dimensional sample of length (or thickness of porous media) ℓ and Δp is the pressure drop. In reality, for an actual filtration system, Eq. (1) is too simple. To predict the flow of two phases (liquid and air) through the media, it is necessary to consider the capillary forces involved as well as the degree of saturation. The total resistance of the bed (R_T), which is equal to (ℓ/k), represents the sum of cake resistance (R_C) and the medium resistance (R_M). Substituting in Eq. (1),

$$U = \frac{Q}{A} = \frac{\Delta p}{\mu(R_\mathrm{C} + R_\mathrm{M})} \tag{2}$$

The value of R_M is usually considered as a constant and not significant when compared with R_C. This assumption is not totally true because the value of R_M increases as the medium blinds. The cake resistance can be replaced by:

$$R_\mathrm{C} = \frac{rWV}{A} \tag{3}$$

where r is the specific resistance, W is the weight of dry solids formed by unit area of filtration, and V is the volume of fluid. Replacing Eq. (3) in Eq. (2), then

$$U = \frac{Q}{A} = \frac{1}{A}\frac{\mathrm{d}V}{\mathrm{d}t} = \frac{\Delta p}{\mu[(rWV/A) + R_\mathrm{M}]} \tag{4}$$

Eq. (4) can be integrated in order to permit correlation of throughput over a finite time [3].

From review of the history in the development of filtration theory, it is interesting to find that the most widely accepted theories aimed at finding the numerical coefficient in the Darcy equation are those based on the concept of hydraulic radius. It has been found earlier that resistance to flow through passages of various noncircular conduits could be brought into agreement with that for circular pipes by employing the hydraulic radius to characterize the respective cross sections. The hydraulic radius, r_H, is defined as

$$r_\mathrm{H} = \frac{\text{cross sectional area normal to flow}}{\text{wetted perimeter}} \tag{5}$$

or

$$r_\mathrm{H} = \frac{\text{volume filled with liquid}}{\text{wetted surface}} \tag{6}$$

Blake [6] was apparently the first to realize that a packed bed might be regarded as a single pipe with a very complicated cross section, and that the interstitial volume could be divided by the wetted packing area to obtain a hydraulic radius. The numerical coefficient in the Darcy equation can be calculated based on the concept that the pore space is equivalent to a bundle of parallel capillaries with a common hydraulic radius and with a cross-sectional shape representative of the average shape of a pore cross section. This development led to what is now known as the Kozeny–Carman equation [7,8]. It is assumed that the path of a streamline through the pore space will be tortuous, with an average length ℓ_e greater than the length of the bed ℓ. Then, the average velocity for viscous flow through any noncircular capillary of hydraulic radius r_H and actual length ℓ_e can be written

$$v_\mathrm{e} = \frac{r_\mathrm{H}^2\,\Delta p}{k_\mathrm{o}\,\mu\,\ell_\mathrm{e}} \tag{7}$$

where k_o is related to the permeability and is equal to 2 for a circular capillary, and the equation then becomes Poiseuille's law.By putting

$$v_\mathrm{e} = \frac{U}{\varepsilon} \tag{8}$$

and from Eq. (6)

$$r_\mathrm{H} = \frac{\varepsilon}{S_\mathrm{v}} \tag{9}$$

where S_v is the particle surface per unit volume of bed (i.e. the specific surface) and ε is the fractional void volume. Thus, we obtain

$$U = \frac{\ell}{\ell_\mathrm{e}}\frac{\varepsilon^3}{k_\mathrm{o}\,\mu S_\mathrm{v}^2}\frac{\Delta p}{\ell} = \frac{\varepsilon^3}{k_\mathrm{k}\,\mu S_\mathrm{v}^2}\frac{\Delta p}{\ell} \tag{10}$$

Here, $k_k = (\ell_e/\ell)k_o$ is known as the Kozeny constant. The ratio ℓ_e/ℓ is called the tortuosity. Later, Carman suggested that the time necessary for fluid to pass through a tortuous track of length ℓ_e is greater than if passed directly through length ℓ by an amount of ℓ_e/ℓ. Hence we obtain the Carman–Kozeny constant as

$$k_{ck} = \left(\frac{\ell_e}{\ell}\right)^2 k_o \tag{11}$$

It has been determined experimentally that $k_{ck} \approx 5.0$ [8]. The Kozeny equation may be expressed in terms of particle size by relating S_v to the particle diameter. For spheres of diameter d, $S_v = 6(1-\varepsilon)/d$, then Eq. (10) becomes

$$U = \left[\frac{\varepsilon^3 d^2}{36(1-\varepsilon)^2 k_{ck}}\right] \frac{\Delta p}{\mu \ell} \tag{12}$$

Here, the expression in brackets is the Darcy constant as shown in Eq. (1).

Generally, the Carman–Kozeny equation has been found to work reasonably well for incompressible cakes over a narrow porosity range, [9] and cannot be used for compressible cakes [3].

2.2. Capillary network model for filter cake

In order to gain a better understanding of the complex transport phenomena that occur in filter cake, a study of the effect of three-dimensional pore geometry on the effective transport properties of the porous media is necessary. Of course, it is known that the agreement will be best if the physical parameters are matched for both model simulation and the actual porous structure. At present, the information from the microscopic pore geometry analysis is not detailed enough to provide an accurate prediction of transport properties for the filter cake from model simulation. Techniques and methodology for a detailed description of the three-dimensional pore structure of a completely interconnected porous system is needed.

Capillary networks, one of the pore structure models, has been used to mimic porous media. For capillary networks, the pore structure is modeled by arrays of capillary tubes. The pore structure of filter cake can be thought to consist of an interconnected three-dimensional network of voids, pores, or capillaries. This three-dimensional network usually has irregular geometry, with different shape and size of capillary segments distributed over the network in irregular fashion. In this regard, it is logical to model capillary pressure curves and other transport properties of filter cake with the help of network models of the pore structure. For example, as shown in Fig. 1, a network model is used to represent the 2-D or 3-D pore structure of a porous medium. The top left-handside of Fig. 1 shows the two-dimensional view of pores whose intersections, the nodes, are numbered. The symbolic graph of this pore structure can be described in the form of a network of bonds and nodes as shown in the top right-handside of Fig. 1. Capillary network models can be used for the prediction of relative permeability and capillary pressure [10,11].

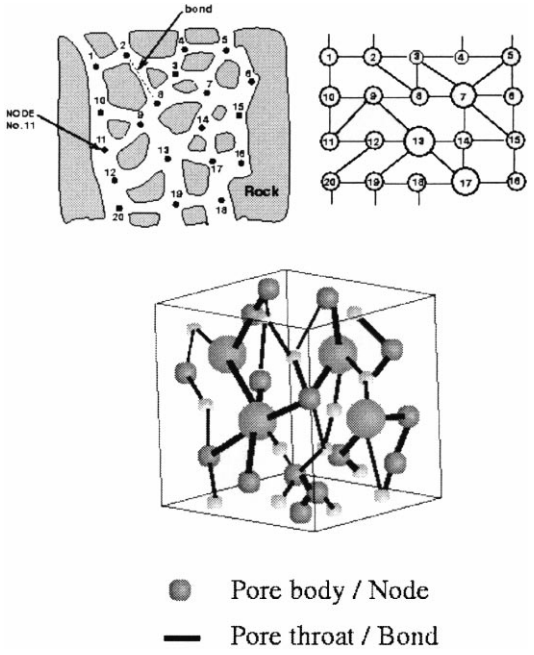

Fig. 1. Symbolic representation of the interconnections in a 2-D [1] and 3-D porous medium.

It is intended to predict the effective transport parameters from microscopic analysis of the three-dimensional interconnected pore structure. To achieve this goal, three major obstacles need to be overcome. First, a reliable and accurate technique for 3-D pore geometry analysis must be established. Second, methodology and procedures for the description of the 3-D interconnected pore structure must be established. Finally, based on this description the last task will be to develop the relationship between the effective transport parameters and the microscopic properties of the pore structure. Of course, model verification is an essential step to confirm any simulation work.

3. 3-D pore geometry analysis by X-ray microtomography

The microstructure and the connectivity of the pore space are important to describe fluid flow in filter cake during fine particle filtration. In this regard, characterization of pore structure based on parameters permitting inferences on the fluid balance is of particular interest. The pore structure has to be described by parameters which are of special relevance for the interpretation of fluid transport phenomena. These parameters should be based on directly measured variables of the pore system and not indirect variables (such as those determined empirically from transport processes) valid only for a particular pore structure. In this way fundamental relationships between pore structure and fluid transport at the

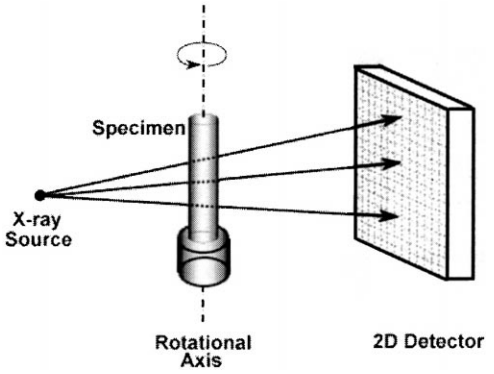

Fig. 2. Schematic diagram of the cone-beam X-ray microtomography system.

microstructure level can be described. In this regard, it is intended to directly measure the three-dimensional interconnected pore structure of the filter cake.

3.1. High resolution X-ray microtomography

Cone-beam X-ray microtomography [12,13] offers a unique imaging capability which can produce three-dimensional images of the internal structure of samples with micrometer resolution. Rather than rotating the X-ray source and detectors during data collection, as in medical CT technology, the specimen is rotated. Instead of generating a series of two-dimensional sliced images from one-dimensional projections, a three-dimensional reconstruction image array is created directly from two-dimensional projections. Fig. 2 shows a schematic diagram for the cone beam geometry micro-CT system. Details for the description of this micro-CT system and its corresponding reconstruction algorithm can be found in the literature [12].

3.2. Sample preparation

To evaluate the effectiveness of the high-resolution 3-D X-ray microtomographic measurement of complex filter cake pore structures, an appropriate specimen was prepared for CT analysis. First, particles, with a size of 210 μm × 150 μm in the density range from 2.65 to 5.0 g/cc, were randomly dispersed in epoxy resin, settled to the bottom and molded into a 7 mm diameter specimen. Then, the specimen was scanned using a cone beam microCT at the University of Michigan. Scanning a specimen takes about 20 min. Full three-dimensional reconstruction requires about 2 h. The reconstruction region of this sample is about 7 mm × 7 mm × 7 mm. The reconstruction set consists of 411 × 383 × 413 points or voxels (volume elements). Thus the voxel size is a cube with sides of 17 μm. Fig. 3 illustrates the co-ordinate system and three slices from different levels of the volume data set for the filter cake specimen.

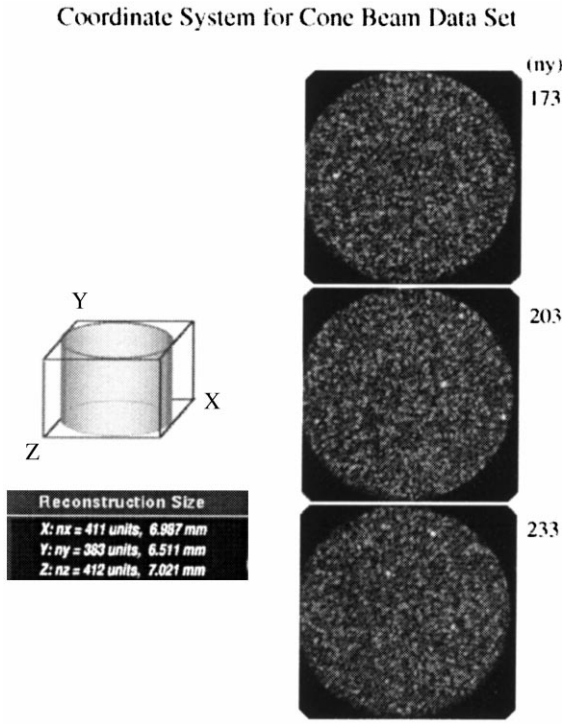

Fig. 3. Coordinate system for the filter cake specimen.

3.3. Pre-processing 3-D cone beam data

The spatial boundary between the pore and the particles can be easily established due to the large difference in densities. Threshold techniques can be used to differentiate and classify the original 3-D density data in order to have higher quality data. In this regard, the 3-D CT data were pre-processed, as shown in Fig. 4, to facilitate the pore geometry analysis. The pre-processing steps are described as follow: (1) cut the 3-D digital data set with the size of 256 × 64 × 256 from original cone beam data (dimension 411 × 383 × 413), (2) threshold the data to obtain binary particle image, and (3) invert the data to obtain binary pore

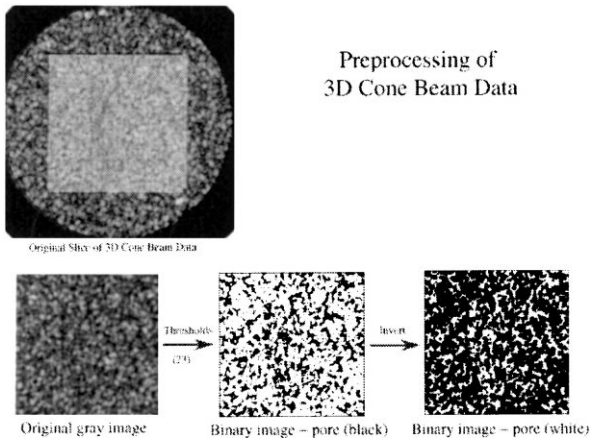

Fig. 4. Pre-processing the cone beam data to extract pore features.

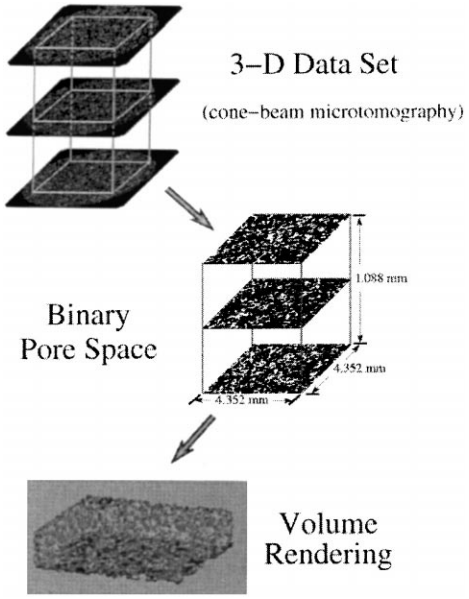

Fig. 5. Schematic diagram for visualization of pore structure from original cone beam 3-D data.

image. Fig. 5 shows the schematic diagram for the construction of the volumetric visualization of pore geometry from the original cone beam data set.

3.4. Volumetric image analysis of pore geometry

Most of the techniques available today for digital image analysis are designed for two-dimensional images. Recent advances in computer technology have made the handling of large data sets feasible. Computers with fast computation speeds and sufficient internal memory is required for the processing of 3-D data sets. The major difference between the analysis of two- and three-dimensional images concerns the aspect on topology. For instance, in 2-D, the algorithm for delineating the object boundary can be easily implemented based on a 'right-hand-on-wall' strategy in which we walk around the object so that the interior always remains to the right until we reach the starting point again. However, in 3-D, the boundary is defined by a surface. There is no obvious strategy for tracing a surface. The following sections discuss some of the basic methods for pore geometry analysis of the volumetric filter cake images.

3.4.1. Porosity, specific surface area, and tortuosity

Porosity, the simplest property of a porous system, is defined as the volume fraction of pores. Specific surface area is defined as the ratio of the surface area of the pores to the bulk volume of the porous medium. The third property, tortuosity, of a porous medium is usually defined as the ratio of the true length of the flow path of a fluid element to the straight-line distance, i.e. the thickness of the filter cake in our case. As mentioned previously in the section of classical filtration theory, the porosity can be used to predict the

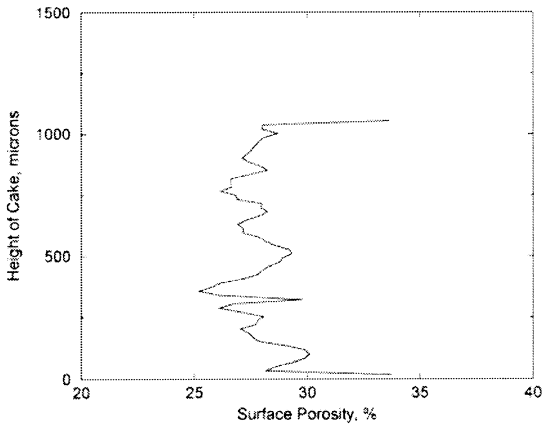

Fig. 6. Surface porosity versus height of filter cake.

permeability defined in Darcy's law as shown in Eq. (12). Porosity, specific surface area and tortuosity of a porous medium, can be used to predict the relative permeability and capillary pressure from pore-scale network modelling.

Quantitative information on porosity and specific surface area of a filter cake can be easily determined from the pre-process binary 3-D data set of the complexed pore structure. The porosity can be measured as the counts of pore voxel (white as shown in Fig. 4) divided by total voxels of the 3-D data set. The specific surface area can be determined as the total number of pore and particle adjacent voxels divided by the total voxel volume. In our case, the total volume and surface area of pore space were determined as $5.4339\,mm^3$ and $190.4512\,mm^2$, respectively, based on the size length of each voxel as $17\,\mu m$. The hydraulic radius obtained from the filter cake was 0.02853 mm. The porosity obtained from the filter cake specimen was 27.7%.

Based on the binary 3-D data set of pore space, the surface porosity can be determined along the depth of the filter cake. The surface porosity is defined as the ratio between void area and the total area of each cross section. The surface porosity with respect to the cake depth is shown in Fig. 6. The surface porosity behavior is similar to the results presented by Brakel and Heertjes [14].

3.4.2. Determination of pore body, pore throats and pore size distribution

Although we can directly access the 3-D pore structure of the porous media with the use of X-ray microtomography, a fundamental difficulty is how to describe the pore structure. In general, the range of pore sizes is very great in most porous media and the geometrical properties of the void system are not easy to define. See Fig. 4. Thus, there is a need for the development of an overall concept for the description of the pore structure. In this regard, it is necessary to develop a capillary network from the 3-D digital map obtained from X-ray microtomography.

Connectivity is an important concept when flow problems are considered. Fluid flow can occur between two points

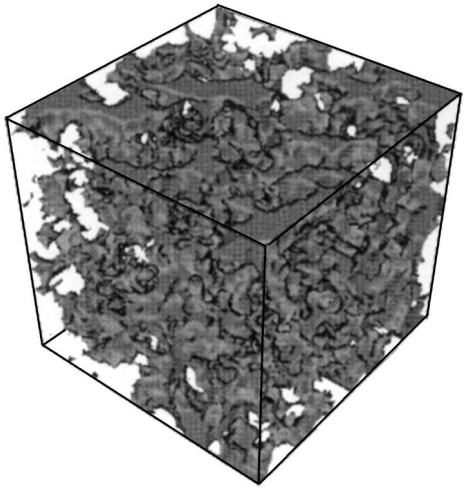

Fig. 7. Surface rendered image of the well connected pore network from subset (64×64×64) of 3-D data set obtained from X-ray microtomography.

only when the pore space is connected. The 3-D interconnected pore structure is difficult to determine by stacking of 2-D thin slices. In addition, to characterize the 3-D interconnected pore structure, the term 'pore size' is not easily defined. These open or interconnected pores can not be simply regarded as discrete pseudo-particles. Several 2-D image processing techniques can be extended to 3-D to characterize the 3-D interconnected pore structure and identify features such as pore body or pore throat. The most important algorithms for 3-D interconnected pore geometry analysis involve connection of components, erosion, dilation, and skeletonization. Connection of components is critical to determine if a particulate feature of pore space is connected or not. Erosion, dilation and skeletonization operations can be used to process and analyze the pore bodies and throats, pore size distribution and interconnected pore structure.

The main concern in volumetric image analysis is the capacity of computer memory. An effective algorithm will be needed such that analysis of the volumetric image can be done sequentially, layer by layer for a huge 3-D digital data set. In this regard, a connection of components algorithm based on the approach by Hoshen and Kopelman [15] was implemented. Although the binary image of the pore space shown in Fig. 4 is not connected, analysis from 3-D connection of components indicates that more than 99% of the pore space belongs to a well connected pore system. Surface rendering of a subset (64×64×64) of this well connected pore network is shown (Fig. 7).

Pore bodies and throats can be obtained with the use of successive morphological operations, erosion and dilation, as described for 2-D [16] and 3-D [17] images. Erosions peel away the outer layer of voxels from the 3-D pore volumes while dilations replace the outer layer. As shown in Fig. 8, for two different sizes of pores, small pores are completely eliminated after two successive erosions without leaving a 'seed' voxel to restore on subsequent dilation. In this manner, the difference of images A and C (A–C) shows the % loss

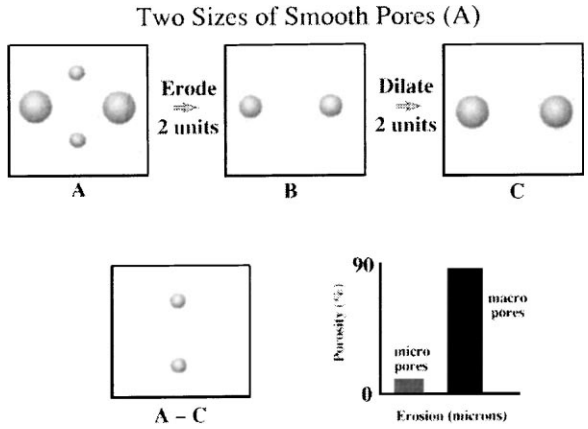

Fig. 8. Schematic representation of pore size measurement using successive erosion/dilation stages.

of pore which is exactly the percent of micropores (number of voxels eroded) in this case.

If two pore volumes are connected by a narrow throat, erosion will break the connections and dilation will restore the pore volume but not re-establish the connection, resulting in a increase in the number of pores and a reduction in average pore size as shown in Fig. 9.

Fig. 10 shows three adjacent slices from the 3-D cone-beam microtomography data for the filter cake specimen converted to a binary image at a voxel intensity threshold level of 23. In this figure the images show the binary porosity (white) following zero, one, and two stages of erosion/dilation (E/D). The small pores or pore throats disappear in successive images with increasing E/D stages until only the large isolated pores remain. Some of these connections which survive the first stage of E/D are shown in the middle column in Fig. 10. In this manner, the largest pore found expressed as a fraction of the total porosity is plotted versus the number of E/D stages [17] as shown in Fig. 11. The original pore structure (no E/D operation) of this filter cake sample has a well-developed pore connectivity. The largest pore found had more than 99% of the

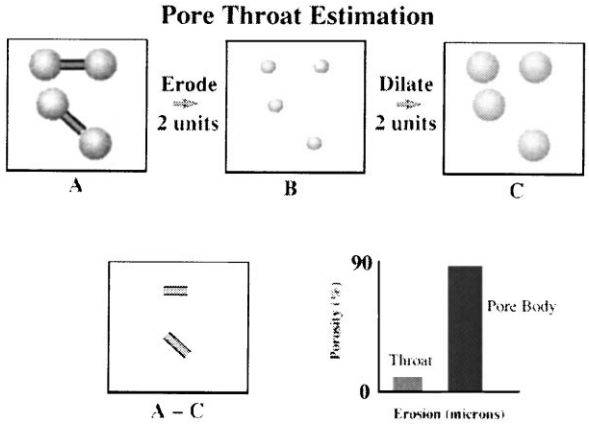

Fig. 9. Schematic representation of estimation of pore body and throat using successive erosion/dilation stages.

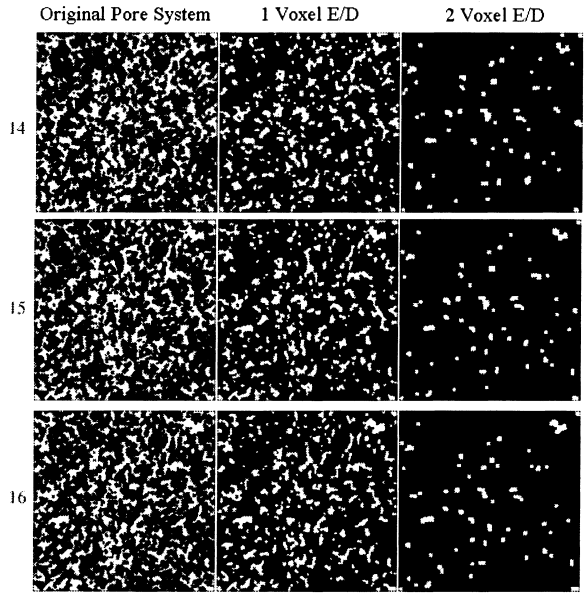

Fig. 10. Three adjacent (14, 15, 16) binary slices of filter cake cone beam micro-tomographic data at a voxel intensity threshold of 23 following zero, one and two successive stages of erosion/dilation (E/D).

total porosity. After one stage of E/D operation, this sample still exhibits of high degree of connectivity implying that the average pore throats approximate two or more voxel dimensions of 17 μm size per voxel for the filter cake sample. After two stages of E/D much of the pore connectivity has been broken for this sample and the results start to approach the isolated pore state shown by the results of Fig. 10. Fig. 12 illustrates the spatial distribution of these isolated pores after two stages of E/D. The pore size distribution based on the equivalent spherical diameter of these isolated pores is shown in Fig. 13.

Since the capillary network will be used to mimic the real filter cake, skeletonization or medial axis techniques [18] should be suitable to build the necessary network and to interpret the linked pore space from the microCT 3-D digital map. Originally, skeletonization (in a plane) denotes a process which transforms a 2-D object into a 1-D graph-like structure, comparable to a stick figure. It is, thereby, essential that the skeleton retains the original connectivity of the shape. Unfortunately, for 3-D objects, there are two different types of skeleton: the medial surface and the medial axis. For instance, the medial surface will be generated using a skeletonization process of a slab object. The skeletonization process provides both the radius information and structure of the object space. This information of 3-D interconnected pore space provides a tool to describe important properties of the completed pore structure and can be used for the capillary network simulation by percolation theory. Several approaches, topological thinning [19–22], distance transformation (DT) [23,24], discrete Voronoi skeletons (DVS) [25], and marching core [26], can be used for algorithm development of the 3-D skeletonization process. The corresponding length and radius of the skeleton segments from the network graph can be used as attributes of the capillary tubes for the

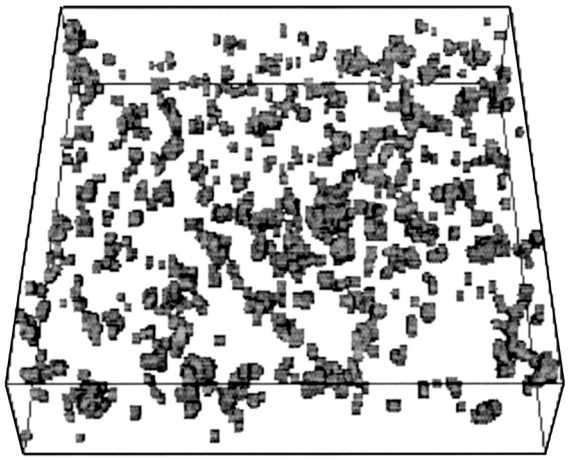

Fig. 12. 3-D view of spatial distribution isolated pores after two stages of E/D.

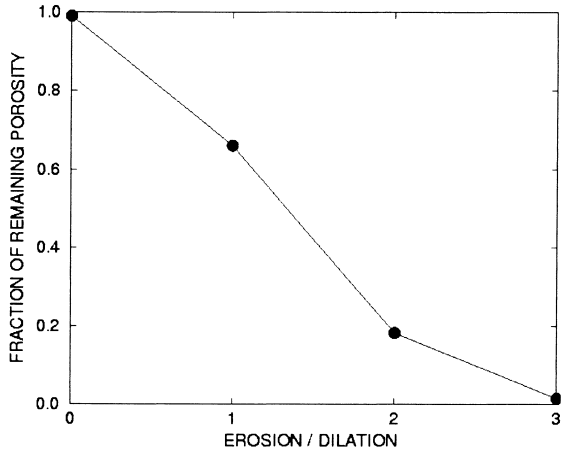

Fig. 11. Largest pore size expressed as a fraction of the total porosity plotted versus number of successive stages of E/D for the filter cake sample.

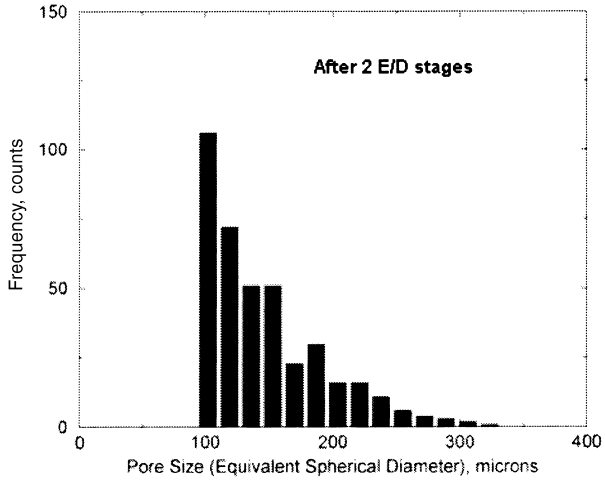

Fig. 13. Pore size distribution after two stages of E/D.

3-D interconnected pore structure. Furthermore, this information can be used to more accurately represent probabilities for the capillary network simulation using percolation theory. Details of the development of 3-D skeletonization and percolation theory will be discussed in a separate contribution.

4. Summary

In order to gain a better understanding of the complex transport phenomena that occur in a filter cake, study of the effect of three-dimensional pore geometry on the effective transport properties in the filter cake is necessary. Algorithms for the processing of 3-D volumetric images to determine the detailed 3-D interconnected pore structure from X-ray microtomography measurements were presented. Pore size measurements on 3-D cone beam X-ray microtomographic data using successive stages of erosion/dilation has revealed information about the connectivity of the filter cake pore structure and allowed for the estimation of pore throat sizes. Most of the pore throat sizes in this particular sample were found to be less than 34 μm. A skeletonization process should provide for better understanding of the pore structure and allow for the interpretation of the interconnectivity. Finally, the capillary network and percolation process should provide the basis for a predictive model to correlate of transport properties of porous media at various scales. Knowledge of multiphase flow in porous media as will be obtained from such a model should provide important information for practical applications in the design of improved filtration processes.

References

[1] F.A.L. Dullien, Porous Media: Fluid Transport and Pore Structure, 2nd Ed., Academic Press, San Diego, CA, 1992.
[2] J. Happel, H. Brenner, Low Reynolds Number Hydrodynamics, Martinus Nijhoff Publishers, Hague, Netherlands, 1983.
[3] L. Svarosvsky, Filtration fundamentals, in: L. Svarosvsky (Ed.), Solid–Liquid Separation, Butterworths, London, 1990, pp. 311–337 (Chapter 9).
[4] D.A. Dahlstrom, C.E. Silverblatt, Continuous vacuum and pressure filtration, in: D.B. Purchas (Ed.), Solid Liquid Separation and Scale Up, Up Lands Press, Croydon, 1977, pp. 445–491.
[5] F.M. Tiller, Filtration Separation 12 (1975) 386.
[6] F.C. Blake, Trans. Am. Inst. Chem. Engs. 14 (1922) 415.
[7] J. Kozeny, Sitz-Ber. Wiener Akad., Abt. IIa, 1927, 136, 271, See also Hydraulik, Springer, Wien, 1953.
[8] P.C. Carman, Fluid flow through granular beds, Trans. Inst. Chem. Engs., London 15 (1937) 150.
[9] S. Ranjan, R. Hogg, The role of cake structure in the dewatering of fine coal by filtration, Coal Preparation 17 (1996) 71–87.
[10] I. Fatt, Trans. AIME Pet. Div. 207 (1956) 144.
[11] P.E. Oren, S, Bakke, N Scandellari, A Henriquez, Prediction of relative permeability and capillary pressure from pore-scale modelling, Proceedings of the 5th European Conference on Mathematics of Oil Recovery, Leoben, 3–6 September 1996, Austria.
[12] L.A. Feldkamp, L.C. Davis, J.W. Kress, Practical cone-beam algorithm, J. Opt. Soc. 1 (6) (1984) 612–619.
[13] C.L. Lin, J.D. Miller, Cone beam x-ray microtomography for three-dimensional liberation analysis in the 21st century, Int. J. Miner. Process 47 (1996) 61–73.
[14] J. Van Brakel, P.M. Heertjes, Homogeneous particle packings and porous masses, some experimental techniques, Powder Technol. 9 (1974) 263–271.
[15] J. Hoshen, R. Kopelman, Percolation and cluster distribution i cluster multiple labeling technique and critical concentration algorithm, Phys. Rev. B 14 (1976) 3438–3445.
[16] R. Ehrlich, S.J. Crabtree, S.K. Kennedy, R.L. Cannon, Petrographic image analysis I. Analysis of reservoir pore complexes, J. Sediment. Petrol. 54 (1984) 1365–1376.
[17] D.A. Doughty, L. Tomutsa, Multinuclear NMR microscopy of two-phase fluid systems in porous rock, Magnetic Resonance Imaging 14 (7) (1996) 869–873.
[18] H. Blum, A transformation for extracting new descriptors of shape, in: Models for the Perception of Speech and Visual Form, MIT Press, Cambridge, MA, 1967.
[19] Y.F. Tsao, K.S. Fu, A parallel thinning algorithm for 3D picture, Computer Graphics Image Processing 17 (1981) 315–331.
[20] W.X. Gong, G. Bertrand, A simple parallel 3D thinning algorithm, Proceedings of the International Conference on Pattern Recognition, 1990, pp. 188–190.
[21] T.C. Lee, R.L. Kashyap, Building skeleton models via 3-D medical surface/axis thinning algorithm, CVGIP 56 (6) (1996) 462–478.
[22] C.M. Ma, M. Sonka, A fully parallel 3D thinning algorithm and its applications, Computer Vision Image Understanding 64 (3) (1996) 420–433.
[23] G. Borgefors, Distance transformations in arbitrary dimensions, CVGIP 27 (3) (1984) 321–345.
[24] N. Gagvani, D. Silver, Parameter Controlled Skeletonization of Three Dimensional Objects, Technical Report CAIPTR216, Rutgers University, June 1997.
[25] R. Ogniewicz, G. Szekely, M. Naf, O. Kubler, Medial manifolds and hierarchical description of 2D and 3D objects with applications to MRI data of the human brain, in: Proceedings of the 8th Scandinavian Conference on Image Analysis SCIA ’93, Tromso, Norway, 1993, pp. 875–883.
[26] J.D. Furst, S.M. Pizer, D.H. Eberly, Marching core: a method for extracting cores from 3-D medical images, in: Proceedings of the Mathematical Methods in Biomedical Image Analysis, San Francisco, CA, June 1996, IEEE Computer Society, pp. 124–130.